Cooperative UAS Geolocation of Emitters with Multi-Sensor-Bounded Timing and Localization Error

Christopher Peters
Electrical and Computer Engineering
Southern Methodist University
P.O. Box 750122
Dallas, TX 75275-0122
228-218-6386
petersc1@mail.smu.edu

Mitchell A. Thornton
Darwin Deason Institute for Cyber Security
Southern Methodist University
P.O. Box 750122
Dallas, TX 75275-0122
214-768-1371
mitch@smu.edu

***Abstract*— A collection of "unmanned aerial systems" (UAS) are wirelessly networked and each is equipped with an antenna, receiver and other components resulting in a cooperative wireless sensor array that can be used for determining RF emitter location estimates. Because each UAS is independently mobile and cooperates with other array elements, the geometry of the wireless sensor array can change in a dynamic manner thus allowing for enhanced accuracy of emitter location estimates through subsequent measurements and iterative location estimate updates. UAS local timing sources and enhanced localization approaches enable time-based emitter location techniques based upon "time-of-arrival" (TOA) or "time-difference-of-arrival" (TDOA) measurements. Sensor localization errors are bounded due to the presence of individual UAS LIDAR ranging subsystems, and the use of new local time source technology likewise bounds the emitter location accuracies due to timing errors. After a review of time-based emitter location methods, two time-based geolocation methods are chosen for this investigation: a multilateration technique and the "Location On a Conic Axis" (LOCA) method. Simulation results predict the accuracy of emitter location estimates versus varying levels of realistic error in array element positioning and time measurements. A study of array size versus emitter location accuracy is also included. The simulation results are compared with the theoretical emitter location accuracy in the presence of the error sources, the Cramér-Rao Lower Bound (CRLB).**

TABLE OF CONTENTS

1. INTRODUCTION

In modern sensing systems across multiple domains, networked "unmanned aerial systems" (UAS) are becoming more common. A collection of UAS with the capability to establish a "wireless ad hoc network" (WANET) results in a cooperative wireless sensor array with a dynamic geometry reconfiguration capability that can be deployed to measure the position of an RF emitter of interest. As an example application, a search and rescue mission might require the ability to obtain the geolocation estimate of an emergency transponder beacon whose location was previously unknown.

It is highly desirable to obtain an estimate of a sensed emitter's location that is accurate and requires as few measurements and computations as possible. This is particularly true when the emitter of interest is transmitting signals of very short time duration. It is well-known that an array's collective Field of View (FOV) with respect to a transmitter location greatly affects emitter location estimates, particularly for time-based emitter location algorithms that are sensitive to the relative geometry of the sensor array and its orientation to the emitter. This motivates the use of a cooperative wireless sensor array since it can be enabled to dynamically reconfigure its array geometry such that iterative measurements cause the emitter location estimate to converge to the true emitter location more quickly and with fewer measurements. A primary motivating factor for choosing a time-based emitter location methodology is the challenge in implementing phase coherence among the array receivers.

The agility and adaptability of a UAS network configured as a cooperative wireless sensor array also offers additional desirable characteristics. When the array is comprised of relatively small UAS (sUAS), search areas that are not possible to navigate with larger fixed-wing aircraft or satellite-based systems, such as confined spaces within a building, underground tunnels, caves, or beneath a foliage canopy, can be practically accessed by the sUAS array. Also, the UAS-based sensor array can operate in hazardous areas such as hostile and radiation- or chemically-contaminated spaces that would otherwise not be accessible for a system requiring human operators aboard.

Although the UAS-based wireless sensor array provides significant advantages in comparison to fixed array systems that may require the presence of human operators, there are technical challenges in designing such a system. One such challenge is that each of the multiple individual sensor apertures is coupled to a different RF receiver, and the apertures are not typically phase coherent since synchronization of the receivers' local oscillators (LO) is

978-1-6654-9032-0/23/$31.00 ©2023 IEEE

difficult to achieve and maintain. The carrying capacity of each UAS can limit the overall allowed payload weight and may require the use of lightweight and less effective onboard assets. Space and weight limitations also restrict the power capacity of onboard batteries, thereby reducing the amount of time that the array can operate before a recharging cycle is required.

In view of these advantages and challenges, the implemented wireless sensor array emitter geolocation techniques should depend on simple and low-power computations while also completing as quickly as possible. Certain other methods of emitter geolocation, such as those that depend upon received signal phase differences or other coherency requirements, such as phase interferometric or cyclostationary approaches, are often impractical to implement. These observations motivate us to consider time-based emitter location approaches that are well-known to have sensitivity to the array geometry and can thus take advantage of the dynamic reconfiguration capability of the array.

"Time of Arrival" and "Time Difference of Arrival" (TOA/TDOA) emitter location methods depend upon solutions of analytical geometry equations in two- or three-dimensions that are defined by the relative positions of the sensor locations and the emitter of interest. In such approaches, emitter location accuracy can be very sensitive to the overall geometry of the array in relation to the true emitter location. The range of the emitter with respect to the sensors is obtained as the product of the timing measurements with the signal propagation speed, typically, the speed of light, c. Due to the large magnitude of electromagnetic signal propagation speed, large changes in the emitter location estimates can occur due to relatively small sensor timing errors or localization errors. For this reason, we are particularly concerned with the effect of these two error sources in a UAS array.

While the local UAS clock sources may be fairly stable and of high frequency through the use of small atomic clocks and accurate frequency multiplication circuitry, the challenge of clock signal synchronization among the array sensors can nevertheless induce timing inaccuracies. Clearly, high-frequency local clock sources are desired to provide as much resolution as possible, and low-drift and jitter are equally important to reduce emitter location estimates due to local timing source inaccuracies.

In the cooperative UAS scenario described here, the UAS positions may be known via the use of the relatively accurate Global Positioning System (GPS) or other navigational systems; however, the UAS comprising the sensor array are individually hovering during the time that TOA/TDOA values are obtained and thus induce a localization error source we term as "hover drift." Other small sensor positioning errors due to variations in environmental factors, such as wind gusts, can cause further degradation in sensor localization. Furthermore, in some environments, GPS may be unavailable requiring an alternative sensor localization approach.

We are motivated to consider the UAS-based cooperative wireless array since the accuracy of emitter location estimates can be partially mitigated using emerging sensor and subsystem technologies that bound the error sources. Specifically, in terms of sensor localization error, we consider the case wherein each UAS incorporates an on-board LIDAR subsystem that permits fine-grained measurements of sensor positioning, such as that described in [1]. Texas Instruments has developed a compact LIDAR solution [2] that permits a ranging accuracy of 1cm at 100m, which is a significant improvement over GPS [3]. For this reason, the positional error of each UAS can be bounded by 2cm. Likewise, in terms of local timing source errors, the emergence of small portable "Chip Scale Atomic Clocks" (CSAC) can provide a basis for a local timing source that is of high resolution and offers low drift and jitter rates [4], [5]. Even without the presence of timing source synchronization methods, the use of a CSAC-based local timing source allows for a free-running timing source that is synchronized at pre-mission time only. Thus, a CSAC-based timing source serves as a reasonable approach to obtain accurate emitter location estimates over limited mission durations. To better characterize the use of such a timing source, we provide simulations that predict the degradation in emitter location accuracy for various levels of timing inaccuracy.

The observations regarding sensor location and local clock source inaccuracies, combined with the use of emerging and recent technology advances, motivates us to analyze the sensitivity and resultant accuracy of the emitter location estimates assuming the presence of the aforementioned technology within the UAS sensor array.

We analyze and describe the impact of these error sources for a cooperative UAS emitter geolocation array using TOA/TDOA methods assuming that error sources are bounded through the use of recent technology. First, we summarize candidate TOA/TDOA-based emitter location techniques to provide context and to justify our choice of emitter location algorithms. Next, we define timing and sensor localization error models and provide simulation results that include the error models. We also formulate and compute the "Cramér-Rao Lower Bound" (CRLB) for emitter location errors that include the presence of the timing and localization inaccuracies to provide an absolute measure of emitter location accuracy. For the simulation analysis, we justify and choose both a TOA-based multilateration and the TDOA-based "Location On a Conic Axis" (LOCA) emitter location algorithm for our wireless sensor array and compare their effectiveness via simulations.

2. TIMING-BASED GEOLOCATION ALGORITHMS

A brief summary of timing-based emitter location approaches is provided as context and to justify our choices for the detailed analysis and simulation efforts. The techniques are described in terms of geometrical concepts. We consider ideal conditions for the description of the emitter location algorithms and address non-ideal conditions in a later section.

Specifically, it is initially assumed that emitter and receiver antennas are omnidirectional within an isotropic wireless channel and that signal propagation speeds, c, are constant. Thus, the underlying geometric principle supporting time-based emitter location algorithms is the resulting spherically-shaped wavefront of the emitter signal as given by the Friis free-space signal power distribution relationship.

In the ideal case, a TOA measurement, t_i, is related to the positions of the i^{th} sensor, s_i, located as a point in three-dimensional space at coordinates (x_i, y_i, z_i) and an emitter similarly located at (x, y, z) as described in (1)

$$t_i = \frac{1}{c}\sqrt{(x - x_i)^2 + (y - y_i)^2 + (z - z_i)^2}. \quad (1)$$

A TDOA measurement, τ_i, corresponding to two sensors, s_i, and s_j is a difference of the two sensors' TOA measurements and is relative to a particular sensor often referred to as the "reference" or "anchor" sensor since the arithmetic subtraction operator is non-commutative. If sensor s_j is designated the reference or anchor sensor, then the TDOA measurement attributed to the sensor pair (s_i, s_j) is expressed as

$$\tau_i = t_i - t_j. \quad (2)$$

Hyperbolic Range Difference Geolocation

A single TDOA value obtained from a pair of sensors at different locations defines a hyperbolic curve with foci coincident to the locations of the sensors and wherein the emitter location is coincident with a point on the hyperbolic curve in a plane defined by the sensor and emitter coordinates that defines a curve of constant TDOA value. Therefore, one method for estimating an emitter location is to use two or more distinct pairs of sensors to likewise obtain two or more distinct hyperbolic curves. Since each hyperbolic curve is coincident with a point representing the position of the emitter of interest, the point at which the hyperbolas intersect defines a unique emitter location estimate. The computational cost for determining the intersection points of two or more hyperbolic curves is significant.

Non-zero timing, sensor localization, and other inaccuracies are always present; therefore, the set of points computed as hyperbolic curve intersections will differ in location. Typically, multiple sensor pairs are deployed to yield multiple TDOA measurements curves that allow for further refining the accuracy of the emitter location through combining all the intersection points. For example, the emitter location estimate can be determined as the point that is as close as possible to all intersection points in a least squared error (LSE) sense.

Lateration-based Geolocation

Lateration-based techniques are based upon finding multiple emitter range estimates for a set of sensors. Each range estimate can be geometrically considered as the radius of a circle in two-dimensional space, or a sphere in three-dimensional space. The emitter location can then be obtained by computing the intersection points of the circles/spheres. Because the range estimates are calculated from TOA measurements, this family of methods is sometimes referred to as "TOA," "circular" or "spherical" techniques.

In the ideal case, a single point of intersection would result, and only two TOA values would be required. Practically, due to the presence of measurement inaccuracies and noise, two TOA measurements result in circles/spheres that do not intersect, that have two intersection points, or that have a "volume" of space for the three-dimensional case. Typically, at least three sensors are deployed. Trilateration, or locating with $n = 3$ sensors, and multilateration, $n > 3$, has been implemented across many domains and continues to be a popular and well-studied topic for range-based localization in wireless networks [6], [7], [8], [9]. For the case of trilateration, three overlapping circles/spheres can yield a small area/volume of common intersection or null intersection. Several approaches for reducing these cases to a single emitter location point estimate have been proffered. For example, one technique involves forming a triangle at each radius point and computing the center of the resulting planar triangle defined by the radius points. The advantage of this method is that an emitter location fix can be obtained regardless of whether the circles/spheres intersect.

The ability to generate and use a plurality of received signal time stamps across many mobile UAS sensors provides the ability to continuously locate and refine an emitter location more effectively than traditional methods. Multilateration systems employ four or more sensors and appropriate methods are used to determine the best-fit emitter location from the resulting multilateral estimates.

In a trilateration approach, the TOA of the emitter signal, t_i, received by the i^{th} sensor, s_i, defines a sphere with a radius equivalent to the range, r_i, of the emitter with respect to the i^{th} sensor. Squaring both sides of (1), expanding, and rearranging yields an expression containing the squared range, $r_i^2 = c^2 t_i^2$, of the emitter to the i^{th} sensor:

$$c^2 t_i^2(t) - x_i^2 - y_i^2 - z_i^2 = x^2 + y^2 + z^2 - 2x_i x - 2y_i y - 2z_i z. \quad (3)$$

Determining the coordinates of the emitter, (x, y, z), requires solving an over-specified system of $n + 1$ equations obtained from n independent TOA measurements. To determine a solution in three dimensions, at least four sensors are required to perform trilateration. An improved emitter location estimate can be obtained with multilateration where $n > 3$ TOA measurements are used.

It was shown in [10] that the series of equations for all sensors can be expressed in matrix representation as

$$\begin{bmatrix} 1 & -2x_1 & -2y_1 & -2z_1 \\ 1 & -2x_2 & -2y_2 & -2z_2 \\ 1 & -2x_3 & -2y_3 & -2z_3 \\ \vdots & \vdots & \vdots & \vdots \\ 1 & -2x_n & -2y_n & -2z_n \end{bmatrix} \begin{bmatrix} x^2+y^2+z^2 \\ x \\ y \\ z \end{bmatrix} = \begin{bmatrix} c^2t_1^2(t) - x_1^2 - y_1^2 - z_1^2 \\ c^2t_2^2(t) - x_2^2 - y_2^2 - z_2^2 \\ c^2t_3^2(t) - x_3^2 - y_3^2 - z_3^2 \\ \vdots \\ c^2t_n^2(t) - x_n^2 - y_n^2 - z_n^2 \end{bmatrix}. \quad (4)$$

Although the matrix and vector components are quadratic, (4) is in the form of a linear equation, $\mathbf{A}_i\mathbf{x} = \mathbf{b}_i$, where matrix $\mathbf{A}$ is formed from the sensor locations and vector $\mathbf{b}$ contains the ranges of the emitter to each sensor. A variety of methods can be employed to solve the over-specified system in (4) as may be found in the literature. The emitter location, (x, y, z), is contained within the solution vector, $\mathbf{x}^{\mathrm{T}} = [x_0 \quad x \quad y \quad z]$. It is noted that the solution to (4) contains an inherent constraint that $x_0 = x^2 + y^2 + z^2$ that is useful for ambiguity resolution in determining the emitter location within $\mathbf{x}$. A common method to solve for $\mathbf{x}$ is to use the pseudo-inverse of $\mathbf{A}$ to provide a minimized L^2 norm solution that results in the LSE solution,

$$\mathbf{x} = (\mathbf{A}^{\mathrm{T}}\mathbf{A})^{-1}\mathbf{A}^{\mathrm{T}}\mathbf{b}. \quad (5)$$

For the multilateration case, a common solution approach is to solve an initial system of four equations with three TOA measurements as a starting point for a "Recursive Least Squares" (RLS) approach by adding each additional TOA measurement and corresponding sensor location to iteratively refine the emitter location estimate.

Lateration-based geolocation can also be employed with TDOA measurements by choosing a reference sensor, s_1, to serve as a "reference" or "anchor" by defining a local coordinate system such that the origin is at the location of the anchor sensor [10]. This effectively converts each sensor's TOA into a TDOA with respect to the anchor sensor. Equation (3) simplifies for the anchor sensor and the range, r_1, of the emitter with respect to the anchor as

$$ct_1 = \sqrt{x^2 + y^2 + z^2}. \quad (6)$$

Following the approach in [11], [12], we square each non-anchor sensor range, $r_i = ct_i$, and subtract from the reference sensor range

$$(ct_i)^2 - (ct_1)^2 = (x_i - x)^2 + (y_i - y)^2 + (z_i - z)^2 + (x_1 - x)^2 + (y_1 - y)^2 + (z_1 - z)^2. \quad (7)$$

The lefthand side of (7) can be rewritten as

$$(ct_i)^2 - (ct_1)^2 = (c\tau_i)^2 - 2tc\tau_i, \quad (8)$$

where the TDOA of sensor s_i with respect to the anchor sensor is denoted as τ_i. Expanding the righthand side of (7) and combining with (8) results in

$$c\tau_i{}^2 - x_1^2 - y_1^2 - z_1^2 - x_i^2 - y_i^2 - z_i^2 = -2(x_1 + x_i)x - 2(y_1 + y_i)y - 2(z_1 + z_i)z + 2c\tau_i\sqrt{x^2 + y^2 + z^2}. \quad (9)$$

Equation (9) is expressed in matrix form as

$$\begin{bmatrix} 2c\tau_2 & -2(x_1+x_2) & -2(y_1+y_2) & -2(z_1+z_2) \\ 2c\tau_3 & -2(x_1+x_3) & -2(y_1+y_3) & -2(z_1+z_3) \\ 2c\tau_4 & -2(x_1+x_4) & -2(y_1+y_4) & -2(z_1+z_4) \\ \vdots & \vdots & \vdots & \vdots \\ 2c\tau_{n-1} & -2(x_1+x_{n-1}) & -2(y_1+y_{n-1}) & -2(z_1+z_{n-1}) \end{bmatrix} \begin{bmatrix} \sqrt{x^2+y^2+z^2} \\ x \\ y \\ z \end{bmatrix} = \begin{bmatrix} c\tau_2{}^2 - x_1^2 - y_1^2 - z_1^2 - x_2^2 - y_2^2 - z_2^2 \\ c\tau_3{}^2 - x_1^2 - y_1^2 - z_1^2 - x_3^2 - y_3^2 - z_3^2 \\ c\tau_4{}^2 - x_1^2 - y_1^2 - z_1^2 - x_4^2 - y_4^2 - z_4^2 \\ \vdots \\ c\tau_{n-1}{}^2 - x_1^2 - y_1^2 - z_1^2 - x_{n-1}^2 - y_{n-1}^2 - z_{n-1}^2 \end{bmatrix}. \quad (10)$$

Equation (10) is now a linear equation in a similar form to (4) and may be solved in a variety of ways including those using the pseudo-inverse and RLS as described in [10].

Location On a Conic Axis

Schmidt [13], [14] developed an approach known as "Location On a Conic Axis" (LOCA) that uses the TDOA of sensor triads to find a straight line corresponding to a conic section axis. TDOA values are converted to range differences that define conic sections wherein the emitter is located at one of the foci and is known to be at a point on a line that is coincident with the conic major axis. In the case of LOCA, the sensor locations are points on the conic and the foci define the emitter location, which is the opposite scenario of hyperbolic geolocation. All conic sections may be considered as defining two foci. In the case of an ellipse or hyperbola, the two foci occupy different and distinct locations. In the case of a circle, the two foci may be considered as being co-located at the same point, and in the case of a parabola, one of the two foci may be considered as having a location that is infinitely distant from the other. Figure 1 contains a diagram of the situation wherein the sensors lie along an ellipse with the emitter being positioned at one of the two distinct focal points.

If the sensor array comprises a total of three elements, the emitter location is computed as a conic section focal point. Since hyperbolas and ellipses have two foci, an ambiguous emitter location point results, and some means must be used for determining which foci corresponds to the actual emitter location estimate. When the sensor array comprises four or more sensors, the emitter location can be computed by considering the intersections of all pairs of lines that define the unique conic axes. Typically, a LSE approach is employed to estimate the emitter location based upon all points formed by intersecting conic axis lines.

The conic axis is derived using (1) in the form of the range of sensor s_i to the emitter,

$$r_i = \sqrt{(x - x_i)^2 + (y - y_i)^2 + (z - z_i)^2}. \quad (11)$$

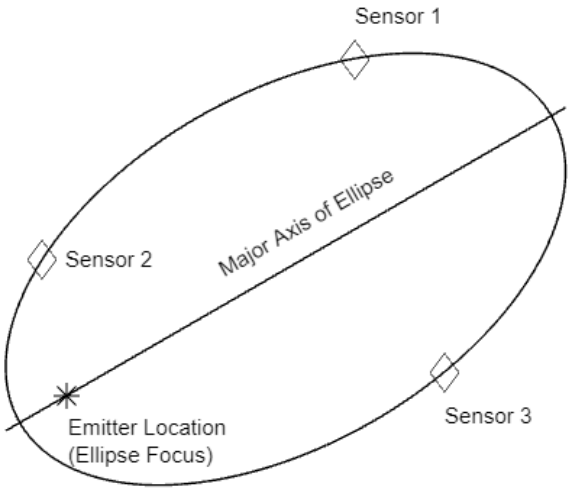

Figure 1. LOCA Positioning finds the Emitter at the focus of an ellipse formed by the range differences of the three Sensors to the Emitter.

We define the difference in two ranges of the emitter with respect to sensors s_i and s_j as Δr_{ij},

$$\Delta r_{ij} = r_j - r_i, \tag{12}$$

and the absolute range, a_i, of each sensor, s_i, with respect to the origin of the coordinate system origin as

$$a_i = \sqrt{{x_i}^2 + {y_i}^2 + {z_i}^2}. \tag{13}$$

We further define Σ as the sum of the range differences as

$$\Sigma = \Delta r_{ij} + \Delta r_{jk} + \Delta r_{ki}. \tag{14}$$

Using a triad of sensors, (s_1, s_2, s_3), the conic axis can be calculated using the range differences as expressed in (12). In three-dimensions, the resulting (15) is expressed in the form of the plane equation, $Ax + By + Cz = D$:

$$\begin{gathered}[x_1\Delta_{23} + x_2\Delta_{21} + x_3(\Delta_{12} - \Sigma)]x + \\ [y_1\Delta_{23} + y_2\Delta_{21} + y_3(\Delta_{12} - \Sigma)]y + \\ [z_1\Delta_{23} + z_2\Delta_{21} + z_3(\Delta_{12} - \Sigma)]z = \\ \tfrac{1}{2}[\Delta_{12}\Delta_{23}\Delta_{31} + {a_1}^2\Delta_{23} + {a_2}^2\Delta_{31} + {a_3}^2(\Delta_{12} - \Sigma)]\end{gathered}. \tag{15}$$

When only three sensors are utilized, an ambiguity can arise when the resulting conic is an ellipse or hyperbola since only one of the two different focal points is the actual position of the emitter. If the conic is a circle or parabola, no ambiguity results. The particular form of the conic resulting from the relative positioning of the sensors and emitter can be determined by computing its eccentricity, e_{cc}. If $e_{cc} = \{0,1\}$, the conic is a circle or a parabola respectively and there is no ambiguity. If $0 < e_{cc} < 1$, the conic is an ellipse and if $e_{cc} > 1$, the conic is a hyperbola. It is noted that the case of all sensors lying along a line can be viewed as a conic section with both foci at infinity and is a degenerate case that is incompatible with the LOCA method. With more than three properly located sensors, ambiguities can be resolved mathematically by including another sensor such that a second independent triad can be formed to compute a second conic thus allowing intersections of the axes of the two conics to be calculated [14]. For the two-dimensional case, two triads (four sensors) are necessary to find this intersection, whereas for the three-dimensional case, since (15) results in the equation of a plane, three triads (at least five sensors) are necessary to find the intersection point. There are $\binom{n}{3}$ triads that can be formed from a set of n sensors. In matrix form, all combinations of triads can be represented as

$$\begin{bmatrix} A_{123} & B_{123} & C_{123} \\ A_{124} & B_{124} & C_{124} \\ \vdots & \vdots & \vdots \\ A_{ijk} & B_{ijk} & C_{ijk} \\ \vdots & \vdots & \vdots \end{bmatrix} \begin{bmatrix} x \\ y \\ z \end{bmatrix} \approx \begin{bmatrix} D_{123} \\ D_{124} \\ \vdots \\ D_{ijk} \\ \vdots \end{bmatrix}, \tag{16}$$

where the A, B, C, and D elements are formed from (15). The (x, y, z) solution to this system of equations, which is the location of the emitter, can be determined with a weighted least squares approach. To perform this computation, each of the A_{ijk}, B_{ijk}, C_{ijk}, D_{ijk} elements in (16) are divided by their respective $\sqrt{{A_{ijk}}^2 + {B_{ijk}}^2 + {C_{ijk}}^2}$ prior to solving (17)

$$\begin{bmatrix} \frac{A_{123}}{\sqrt{{A_{123}}^2+{B_{123}}^2+{C_{123}}^2}} & \frac{B_{123}}{\sqrt{{A_{123}}^2+{B_{123}}^2+{C_{123}}^2}} & \frac{C_{123}}{\sqrt{{A_{123}}^2+{B_{123}}^2+{C_{123}}^2}} \\ \frac{A_{124}}{\sqrt{{A_{124}}^2+{B_{124}}^2+{C_{124}}^2}} & \frac{B_{124}}{\sqrt{{A_{124}}^2+{B_{124}}^2+{C_{124}}^2}} & \frac{C_{124}}{\sqrt{{A_{124}}^2+{B_{124}}^2+{C_{124}}^2}} \\ \vdots & \vdots & \vdots \\ \frac{A_{ijk}}{\sqrt{{A_{ijk}}^2+{B_{ijk}}^2+{C_{ijk}}^2}} & \frac{B_{ijk}}{\sqrt{{A_{ijk}}^2+{B_{ijk}}^2+{C_{ijk}}^2}} & \frac{C_{ijk}}{\sqrt{{A_{ijk}}^2+{B_{ijk}}^2+{C_{ijk}}^2}} \\ \vdots & \vdots & \vdots \end{bmatrix} \begin{bmatrix} x \\ y \\ z \end{bmatrix} \approx \begin{bmatrix} \frac{D_{123}}{\sqrt{{A_{123}}^2+{B_{123}}^2+{C_{123}}^2}} \\ \frac{D_{124}}{\sqrt{{A_{124}}^2+{B_{124}}^2+{C_{124}}^2}} \\ \vdots \\ \frac{D_{ijk}}{\sqrt{{A_{ijk}}^2+{B_{ijk}}^2+{C_{ijk}}^2}} \\ \vdots \end{bmatrix}. \tag{17}$$

3. GEOLOCATION INACCURACY SOURCES

This section describes some of the dominant error sources present in the cooperative wireless sensor array comprised of UAS equipped with individual antennas, RF receivers, local positioning means, high-resolution timers, WANET interfaces and computing subsystems.

In the previous Section the location of each sensor, s_i, is modeled as its true location with three-dimensional coordinates (x_i, y_i, z_i). Practical emitter location systems such as those described in this paper always operate with measurement inaccuracies associated with sensor localization. Thus, a better model for the current location of each sensor, s_i, is to consider the coordinates,$(\hat{x}_i, \hat{y}_i, \hat{z}_i)$, that include error terms, $(\varepsilon_x, \varepsilon_y, \varepsilon_z)$, as given in (18):

$$\hat{x}_i = x_i + \varepsilon_{xi}, \quad \hat{y}_i = y_i + \varepsilon_{yi}, \quad \hat{z}_i = z_i + \varepsilon_{zi}. \tag{18}$$

Assuming the signal propagation velocity, c, is constant in a particular environment, the emitter range is dependent on the accuracy of the emitter-to-sensor propagation time. It would be preferable if the local UAS clock sources within the wireless array network could operate in a synchronous manner at precise and equal frequencies with minimal drift to enable phase coherency among the array elements; however, this is a difficult condition to achieve and is not considered to be an option in this study. Even when the local UAS clocks are synchronized prior to the emitter location mission, the presence of clock drift and jitter will affect timing accuracy and would thereby cause degradation in RF emitter localization estimates. The sensor TOA measurement can be modeled as the true TOA, t_i, with a corresponding error term, ε_{ti}, as

$$\hat{t}_l = t_i + \varepsilon_{ti}. \tag{19}$$

If each UAS comprised a GPS receiver as a means of a local clock source, the provided GPS time reference signal is accurate to 30ns [3]. However, when GPS is unavailable within the dynamic environment of a UAS mission, or, if the UAS are not equipped with GPS receivers, the utilization of a WANET clock synchronization method would be desirable to mitigate clock error. It is shown in [15] and [16] that, with a wideband receiver, it is possible to measure propagation time at sub-nanosecond accuracy using off-the-shelf IEEE 802.11 Wi-Fi network interface cards. The use of Ultrawideband (UWB) in [17] was shown to achieve sub-nanosecond accuracy. The application of such an approach to the cooperative wireless sensor network described here could result in a clock synchronization accuracy approaching 1ns. Another significant advancement in local timing sources is the emergence of "Chip Scale Atomic Clocks" (CSAC) that provide highly stable and accurate timing sources with a small form factor [4], [5], [18], [19]. The use of a CSAC with a companion high-accuracy frequency multiplier such as an *LC*-based "voltage- or current-controlled oscillator" (VCO/ICO) should allow a local clock source of 1 GHz with a highly stable characteristic to be deployed on each UAS. Each CSAC-based timing source could be augmented with synchronization methods or used in a free-running approach for limited mission lifetimes. Our simulation results contain a range of local UAS clock error levels that include both these higher-accuracy conditions as well as more degraded or larger local clock errors so that all of these possibilities are included for consideration.

Other error sources and measurement inaccuracies can additionally affect the accuracy of the emitter location estimates. The assumption of constant signal propagation velocity neglects atmospheric refraction effects. Additionally, signal fading effects due to Rayleigh scattering and the presence of multipath may affect location accuracies. Multipath is of particular concern when the sensor array is deployed within a dense urban environment that may consist of large metallic structures such as the steel frames of large buildings. The UAS-based wireless system considered here is assumed to be operational in the far-field but at relatively short ranges to the emitters, thus, the multipath effects are probably the more dominant contributors among this group. The incorporation of dynamically updated signal propagation speed and the use of models that predict multipath effects such as a Rician propagation model could be optionally included in the sensor array if sufficient WANET bandwidth and a reliable means for estimating the signal propagation characteristics were present. In this study, we assume that these resources are not present. It is likewise assumed that the detected and received RF transmissions of each sensor are at sufficiently high-power levels such that variations in antenna gain patterns are negligible and that all sensors receive transmitted emitter signals at sufficiently high "Signal-to-Noise" (SNR) levels. For these reasons, we only focus on array element localization and local measurement timing errors.

Another significant source of inaccuracy is related to the ability of each sensor to accurately identify the same instantaneously received signal features when obtaining a TOA measurement by assigning a local time stamp to the same portion of the received signal by each sensor array element. This issue has been addressed in depth in past work. For communications signals, correlation calculations are generally used to find time-stamping signal locations [20], [21], [22], [23], [24]. Whereas for pulsed signals, rising or falling edges are typically used [25], [26] to more accurately determine TOA signal time stamps. It is assumed that this "time stamping" error source is relatively small in comparison to the error contributions due to the case where local UAS timing sources are asynchronous with respect to one another. That is, it is assumed that any timing errors due to misaligned time stamping of received signal artifacts among individual sensor array elements is much less than the local UAS clock period. Thus, inaccuracies due to this error source may be considered as being contained within the timing error models employed in our analyses.

4. CRAMÉR-RAO LOWER BOUND FOR SENSOR POSITION AND CLOCK TIMING ERRORS

In consideration of the dominant error sources due to sensor localization caused by UAS hover drift and the fact that local clock sources with errors are present within each UAS, we model the cooperative wireless sensor array network and simulate the resulting emitter location accuracy with these error sources present using different timing-based emitter location algorithms. Specifically, we consider both multilateration and LOCA emitter location techniques in our models.

To provide a unified basis in evaluating the emitter location accuracy of the sensor array, we also derive and compute the Cramér-Rao Lower Bound (CRLB) to evaluate the theoretically possible emitter location accuracy due to varying amounts of the dominant sources of error and measurement inaccuracy.

The CRLB is a measure of the minimal variance that can be achieved by an unbiased estimator. The positions of the UAS are known to a certain accuracy characterized by the standard deviations of the location estimates, $(\sigma_{xi}, \sigma_{yi}, \sigma_{zi})$. Likewise, the local timing errors within each UAS are modeled with a standard deviation statistic denoted as σ_{ti}. The measurement errors are modeled as Gaussian "Random Variables" (RV), following the approaches in [27], [28], [29], [30] with a likelihood function of:

$$p(\hat{\tau}_l|\mathbf{x}) = \frac{1}{\sqrt{2\pi}\sigma_i} e^{-\frac{1}{2{\sigma_i}^2}\left(\hat{\tau}_l - \tau_i(\mathbf{x})\right)^2}. \quad (20)$$

With respect to TOA measurements, we assume that the variance of a single measurement is dependent on the variance ${\sigma_i}^2$ of the single sensor s_i. For TDOA approaches, [29] and others show that the use of the common reference or anchor sensor, s_1, correlates the measurements so that the variance of a single measurement is the sum of the variance of the two sensors, ${\sigma_i}^2 + {\sigma_1}^2$, as characterized by the corresponding $\{n-1\} \times \{n-1\}$ covariance matrix:

$$\boldsymbol{R}_{TDOA} = \begin{bmatrix} {\sigma_2}^2 + {\sigma_1}^2 & {\sigma_1}^2 & \cdots & {\sigma_1}^2 \\ {\sigma_1}^2 & {\sigma_3}^2 + {\sigma_1}^2 & \cdots & {\sigma_1}^2 \\ \vdots & \vdots & \ddots & \vdots \\ {\sigma_1}^2 & {\sigma_1}^2 & \cdots & {\sigma_n}^2 + {\sigma_1}^2 \end{bmatrix}. \quad (21)$$

The CRLB is determined by calculating the inverse of the Fisher Information Matrix (FIM), $\mathbf{J}$, expressed as

$$\mathbf{J} = E\{\nabla_{\mathbf{x}} \ln p(\hat{\tau}_l|\mathbf{x}) \, (\nabla_{\mathbf{x}} \ln p(\hat{\tau}_l|\mathbf{x}))^{\mathrm{T}}\}, \quad {\sigma_i}^2 \geq \mathbf{J}^{-1}. \quad (22)$$

$E\{\cdot\}$ denotes the expected value operator of a RV. Under the assumption that the errors are modeled with a Gaussian RV, a constant covariance matrix results [29]. The elements of the FIM can be determined as

$$\mathbf{J}_{ij} = \left(\frac{\partial \tau(\mathbf{x})}{\partial x_i}\right)^{\mathrm{T}} {\mathbf{R}_{TDOA}}^{-1} \left(\frac{\partial \tau(\mathbf{x})}{\partial x_j}\right), \quad \frac{\partial \tau(\mathbf{x})}{\partial x_i} = \begin{bmatrix} \frac{\partial \tau_2(\mathbf{x})}{\partial x_i} \\ \frac{\partial \tau_3(\mathbf{x})}{\partial x_i} \\ \vdots \\ \frac{\partial \tau_n(\mathbf{x})}{\partial x_i} \end{bmatrix}. \quad (23)$$

For receiver localization errors, the FIM becomes

$$\mathbf{J}_{\tau} = \begin{bmatrix} \frac{\partial \tau_2}{\partial x} & \frac{\partial \tau_3}{\partial x} & \cdots & \frac{\partial \tau_n}{\partial x} \\ \frac{\partial \tau_2}{\partial y} & \frac{\partial \tau_3}{\partial y} & \cdots & \frac{\partial \tau_n}{\partial y} \\ \frac{\partial \tau_2}{\partial z} & \frac{\partial \tau_3}{\partial z} & \cdots & \frac{\partial \tau_n}{\partial z} \end{bmatrix} {\mathbf{R}_{TDOA}}^{-1} \begin{bmatrix} \frac{\partial \tau_2}{\partial x} & \frac{\partial \tau_2}{\partial y} & \frac{\partial \tau_2}{\partial z} \\ \frac{\partial \tau_3}{\partial x} & \frac{\partial \tau_3}{\partial y} & \frac{\partial \tau_3}{\partial z} \\ \vdots & \vdots & \vdots \\ \frac{\partial \tau_n}{\partial x} & \frac{\partial \tau_n}{\partial y} & \frac{\partial \tau_n}{\partial z} \end{bmatrix}^{\mathrm{T}}. \quad (24)$$

The FIM can be evaluated in the temporal (time) domain or in the spatial (range) domain depending on the error terms of the covariance matrix. The conversion to the range domain is obtained by multiplying ${\mathbf{R}_{TDOA}}^{-1}$ with the square of the signal propagation speed, c^2. In the following analysis, the receiver location error contributions are analyzed in the range domain using (6) and (11).

For timing errors, [17], [29], [30] identified the primary contributing factor for calculating the CRLB of a TDOA estimate to be the bandwidth, B, of the received signal and the received signal SNR_i at sensor s_i, via the relationship:

$${\sigma_i}^2 \geq \frac{c^2}{B^2 * \mathrm{SNR}_i}. \quad (25)$$

Following [29], we consider the factors carrier frequency, bandwidth, integration time, propagation velocity, *etc*. to be incorporated into the constant, a. Note that the received signal SNR_i at the i^{th} sensor element is not considered within the constant, a, in our analysis since we assume that SNR_i exceeds a threshold value. That is, we assume that the received signal is at a sufficiently high SNR to enable emitter location estimation such that a need not comprise a contribution due to SNR_i. Because the SNR_i of the emitter at s_i is inversely proportional to the range by $\frac{1}{r^2}$, an ideal lower threshold for the distance, r_0, for an optimal SNR_0 is used to determine the SNR_i, by:

$$\mathrm{SNR}_i = \mathrm{SNR}_0 \frac{{r_0}^2}{{r_i}^2}. \quad (26)$$

The associated variance is then:

$${\sigma_i}^2(r) \geq \frac{a}{\mathrm{SNR}_0} * \frac{{r_i}^2}{{r_0}^2}. \quad (27)$$

As an example of this effect, we assume a signal bandwidth, B, and corresponding SNR_0 that result in a worst case, or maximum value, for the standard deviation, σ, to be approximately 1ns at the maximum range. Figure 2 shows the improvement of σ for increasing SNR where the minimum σ is determined by the SNR at r_0.

Following [29], because the variance is range-dependent and

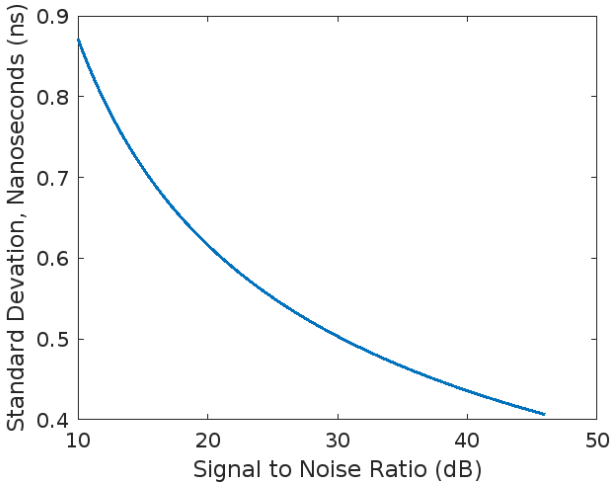

Figure 2. Standard Deviation of local timing inaccuracy as a function of SNR.

no longer constant, its term in the likelihood function, and therefore the FIM, is not reduced. The TDOA sensor pair ${\sigma_i}^2 + {\sigma_1}^2$ variance term is:

$$ {\sigma_i}^2 + {\sigma_1}^2 = \frac{a({r_i}^2 + {r_1}^2)}{{r_0}^2 \mathrm{SNR}_0}, \tag{28} $$

with a standard deviation, σ_{i1}, given by

$$ \sigma_{i1} = \sqrt{{\sigma_i}^2 + {\sigma_1}^2} = \frac{\sqrt{a({r_i}^2 + {r_1}^2)}}{r_0 \sqrt{\mathrm{SNR}_0}}. \tag{29} $$

The FIM in (22) takes the form

$$ \mathbf{J}_{ij} = \left(\frac{\partial \tau(\mathbf{x})}{\partial x_i}\right)^{\mathrm{T}} \mathbf{R}(\mathbf{x})^{-1} \frac{\partial \tau(\mathbf{x})}{\partial x_j} + \frac{1}{2} tr\left(\mathbf{R}(\mathbf{x})^{-1} \left(\frac{\partial \sigma_{i1}}{\partial x_i}\right)^{\mathrm{T}} \mathbf{R}(\mathbf{x})^{-1} \frac{\partial \sigma_{i1}}{\partial x_j}\right), \tag{30} $$

with a parameter-dependent FIM Jacobian of

$$ \frac{\partial \sigma_{i1}}{\partial \mathbf{x}} = \frac{\sqrt{a}(\mathbf{r}_i + \mathbf{r}_1)}{r_0 \sqrt{\mathrm{SNR}_0 ({r_i}^2 + {r_1}^2)}}. \tag{31} $$

Using the FIMs in (24) and (30), as substituted into (22), allows for the computation of the TDOA CRLB that encompasses inaccuracies due to array element localization error and local timing variances, respectively. Considering the LOCA emitter location technique, the analysis considers a combination of sensor triads instead of using a single reference or anchor sensor; thus, the covariance matrix in (21) evolves to the cases for considering the individual sensor triads. There is an expected processing gain as the number of sensors is increased since the result is dependent on the intersection of all the resulting planes. Our analysis is based on a least squares method to reduce the TDOA and LOCA results; however, many approaches exist to improve the TDOA accuracy through other processing methods or specialized geometries [31].

5. SIMULATIONS

Models are formulated wherein sensor networks of fixed-location UAS are used to determine the location of a small, stationary emitter transmitting a 5GHz signal. In these simulations, the transit time of sensed signals to each UAS receiver is used to find the emitter ranges, and the solution algorithms in (4) and (17) calculate the emitter location. The geometry assumed all sensors to be in the far-field of the stationary emitter, and the simulations varied the number of receivers and varied the locations of the sensors and emitter. The receivers are randomly distributed within a range of 200m from the emitter, following a uniform distribution, for 100 unique geometries. The reference or anchor sensor is always placed at the origin, as shown in Figure 3 for a geometry of five sensors. While a primary motivation for deploying a cooperative and wireless sensor array to locate emitters is due to the ability to dynamically reconfigure the array geometry and to improve emitter location accuracy through subsequent measurements, we choose to consider the case where only a single emitter location estimate is performed at each simulated time instance to capture worst-case behavior. Iteratively updating the emitter location estimate by including subsequent measurements will greatly improve system accuracy, particularly when new geometries are used that enhance the new FOV in relation to the previous FOV.

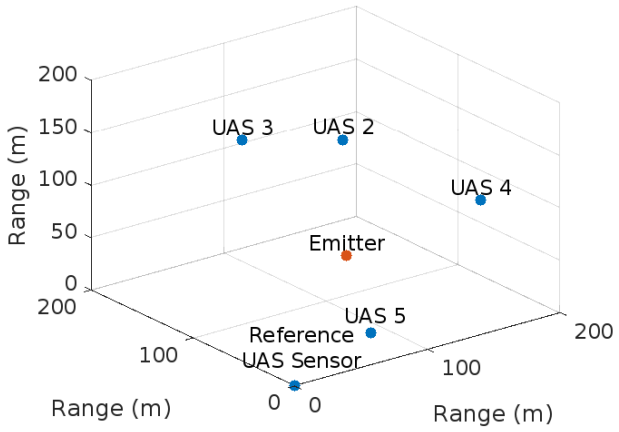

Figure 3. Example sensor geometry for five UAS sensors

The true location of the emitter is randomly selected for 100 unique geometries. The number of receivers varies from 5 to 25 to show the improvement in emitter location with increasing array size. We use Monte Carlo simulations with 10,000 runs (*i.e.*, 100 emitter geometries with 100 sensor geometries each) for our analysis. The same geometry, both in terms of quantities and locations, of each run was processed with both the LOCA and TDOA algorithms to avoid geometry bias in the comparisons of the two emitter location techniques. The RMS error distribution of the error-free solutions for each of the TDOA and LOCA algorithms is provided in Figure 4 and, as is expected, Figure 5 indicates that the error values improve in a roughly logarithmic manner with increasing sensor quantities. Although it is certainly dependent upon the specific mission objectives, it is generally observed that array sizes of five to ten sensors should be sufficient for most applications.

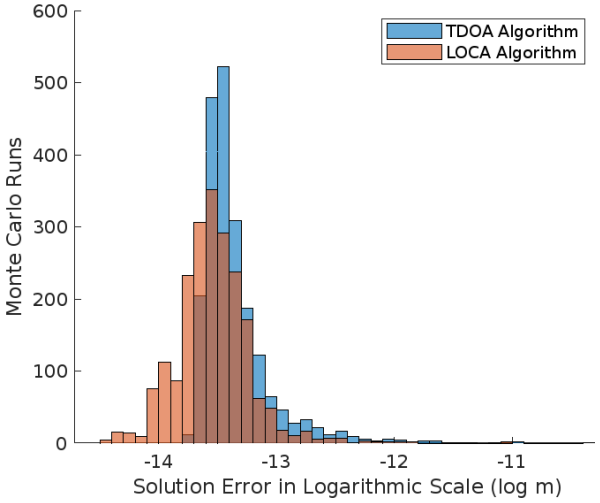

Figure 4. Histogram of RMS error of TDOA and LOCA algorithms with no induced error.

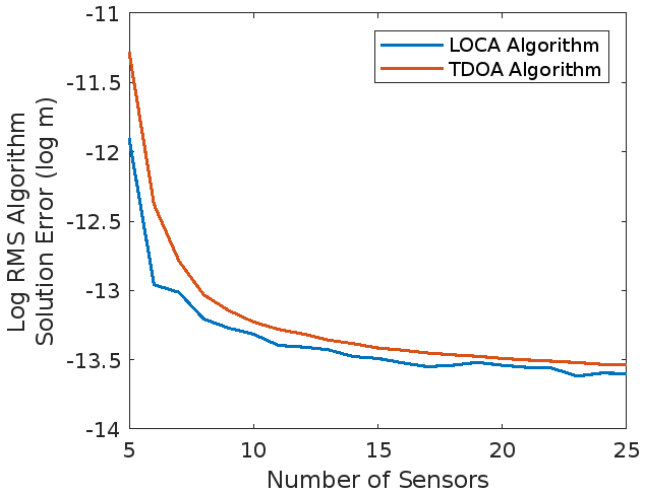

Figure 5. RMS error of TDOA and LOCA algorithms with no induced error for increasing sensor quantities.

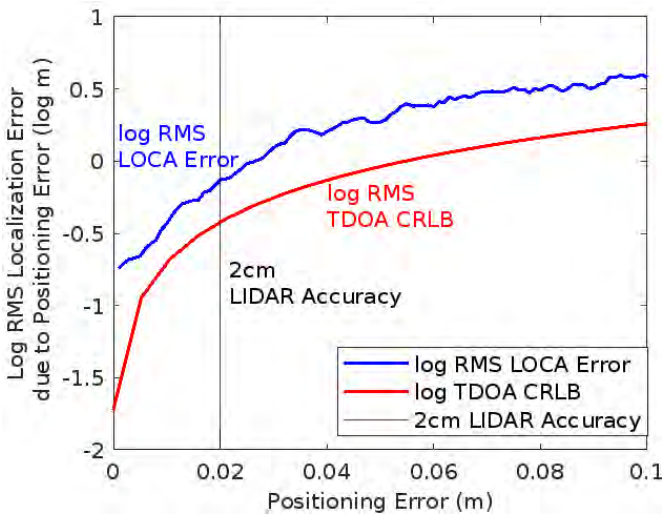

Figure 6. Log RMS localization error of LOCA algorithm with increasing sensor positioning error, upper-bounded by in-network sensor positioning accuracy.

6. RESULTS

Unless otherwise noted in the description of the simulation results, we assume that the local sensor timing sources are initially synchronized prior to mission initiation. We then set the timing source inaccuracy to have a standard deviation of 1ns due to the justifications previously described. Likewise, due to the use of local sensor LIDAR ranging, the locations of each sensor are assumed to be known within an accuracy of 2cm. Localization and timing errors are incorporated in a manner consistent with the assumptions that result in (18) and (19). More specifically, the errors are modeled as Gaussian-distributed RVs with respect to the sensor range values that are used in the emitter location algorithm. These simulation results are then compared to the CRLB results to obtain an estimate of overall performance.

The sensor position inaccuracy is varied versus increasing sensor array size using the signal parameters discussed in Section 5. Figure 6 illustrates the impact of an increasing sensor positioning error and shows how the error of the emitter location estimate increases as sensor positioning error increases. If the sensors are localized with an intra-array method such as LIDAR, then the localization error has an upper-bound to the accuracy from that sensor positioning method, which is 2cm in this case. The availability of practical LIDAR ranging subsystems within individual sensor elements greatly impacts the viability and practicality of using a collection of UAS to serve as a cooperative wireless sensor array for the purpose of estimating an RF emitter location since it provides an upper bound on array element localization error. Figure 7 contains simulation results in the form of RMS emitter range error due to sensor positioning errors, on a logarithmic scale, versus varying numbers of sensor array elements for a given array geometry. Specifically, the range error in Figure 7 is the RMS Euclidean distance from the true emitter location to the estimated emitter location for each measurement.

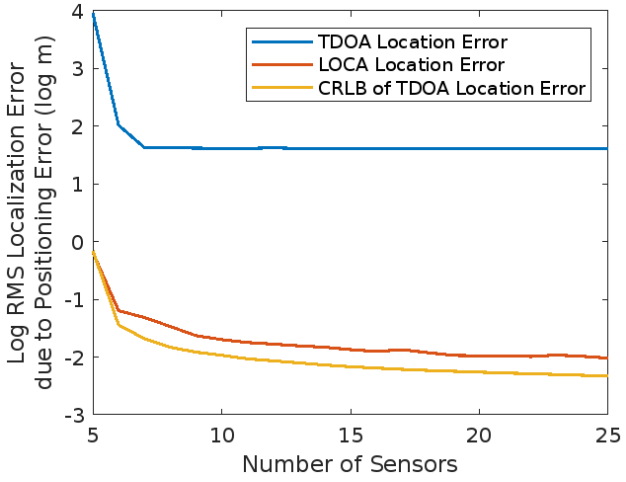

Figure 7. RMS error of TDOA and LOCA algorithms with induced sensor positioning error for increasing sensor quantities.

For the multilateration technique (referred to as "TDOA Location" in Figure 7), the overall absolute error in emitter location range is much higher than the CRLB, while the same error for LOCA is much closer to the CRLB. As expected, the impact of sensor positioning decreased with more sensors and as also expected, the RMS emitter location range error varies and depends upon array geometry. Although a variety of different randomly-selected array geometries are analyzed, only a single representative example is included in this paper. There is a noticeable accuracy improvement for LOCA as the number of sensors increases, whereas for the multilateration, or TDOA algorithm, the induced errors diminish the processing gains found with increasing sensor quantities when the array size exceeds eight sensors.

The local sensor timing error is also simulated for increasing numbers of array elements using the same geometries and

signal parameters as discussed in Section 5. Figure 8 contains mean RMS emitter location error, on a logarithmic scale, due to local sensor timing offsets versus an increasing sensor array size. Consistent with the results due to sensor localization inaccuracies, the multilateration, or TDOA, error is significantly higher than the CRLB, whereas the LOCA error is significantly closer to the CRLB. Again, there is an accuracy improvement with LOCA as the number of sensors increases, whereas the TDOA error remains nearly constant. Therefore, we reach the same conclusion that, although highly dependent upon mission parameters, an array size in excess of eight sensors provides largely diminishing increases in emitter location accuracy.

Local sensor element timing inaccuracies and their result on emitter location accuracy is simulated for several different values of timing accuracy using the LOCA method and are provided in Figure 9.

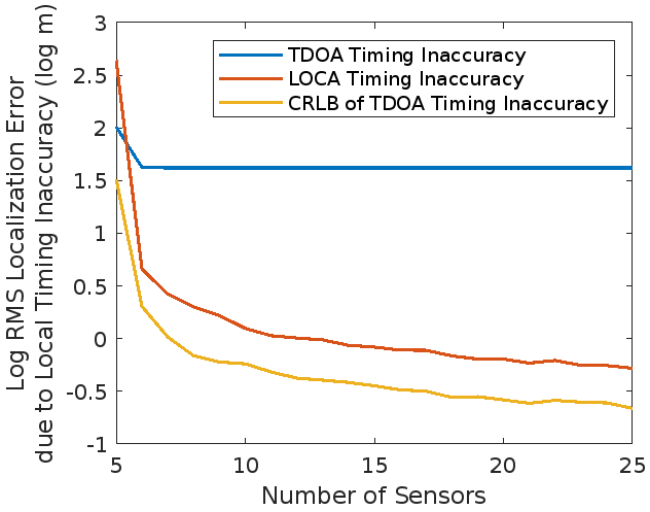

Figure 8. RMS error of TDOA and LOCA algorithms with induced local timing inaccuracy for increasing sensor quantities.

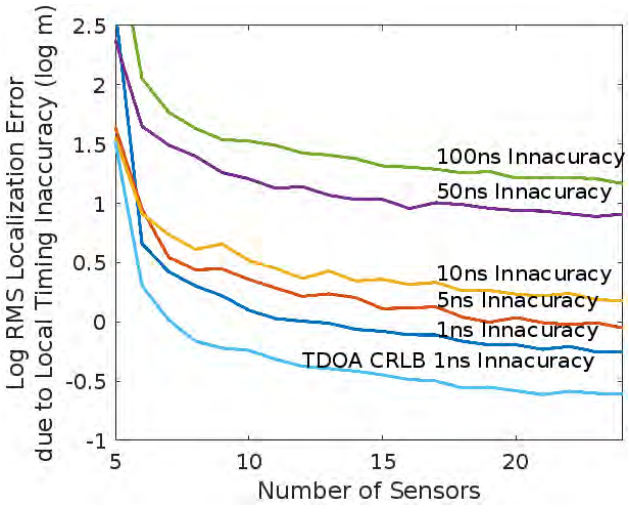

Figure 9. RMS error of LOCA algorithms with varying induced local timing inaccuracy for increasing sensor quantities.

It is concluded that the cooperative use of increasing numbers of sensors in the UAS network can overcome the local timing inaccuracies to a certain extent if the previously assumed 1ns bound on timing errors is not achievable in a geometry. As shown in Figure 2, as the overall mean range of the UAS array position to that of the true emitter location decreases, the received signal SNR_i at each sensor increases. If available, the utilization of array clock synchronization methods decreases the emitter location error, and the emitter location resolution will increase. In this case, since local timing source synchronization is likely an expensive operation, a larger array size with less accurate timing sources can be used to obtain an initial emitter location estimate. Next, a timing source synchronization operation among a smaller subset of array elements can be used to obtain a subsequent emitter location estimate that is more accurate and that could potentially be acquired in a closer range to the emitter position. Furthermore, the initial emitter location estimate could be used to select the subset of array elements to be synchronized, a new geometry for those elements, and even the choice of an alternative emitter location algorithm to be used for subsequent measurements.

7. CONCLUSION

We are motivated to consider the use of a cooperative wireless sensor array comprised of a collection of UAS that contain onboard assets permitting them to operate as an emitter location system. Our primary motivation is due to the fact that the array geometry can be dynamically updated and reconfigured for subsequent iterative emitter location measurements thus potentially providing a large advantage in comparison to conventional fixed-array systems. Another major motivation for the use of a collection of UAS as an emitter location system is the availability and practicality of including other onboard sensors and subsystems such as LIDAR ranging and accurate local timing sources that allow for measurement accuracies to be bounded. The example that is investigated here is the use of LIDAR ranging to bound sensor localization errors.

As a preliminary investigation into the viability of this approach, we focus on analysis of the dominant error sources within the system. We justify our selection of the dominant error sources through inclusion of a summary of several error sources and how these errors can be minimized or mitigated. Specifically, these include errors due to local timing measurements and array element positioning errors. These dominant error sources are analyzed through the use of the theoretical lower bound on accuracy using the CRLB and in terms of the use of multilateration and LOCA emitter location algorithms.

Our analysis also includes an investigation into the required number of sensor array elements, and we conclude that, although specific mission parameters may affect the choice of element numbers, a network of more than eight elements tends to provide diminishing improvements in terms of emitter location for most mission profiles. Due to difficulties

in local timing source synchronization, we also focus on timing-based emitter location algorithms here and provide a brief summary of their functionality. We also describe how timing error can be bounded through the use of a variety of techniques ranging from the use of UWB methods for very small error bounding, to the use of GPS for an increased error bound, and up to the use of sources that are merely synchronized during the pre-mission preparation and then run freely during the mission's lifetime.

We conclude that such a system is viable and practical, particularly with the inclusion of fused data from other sensors to provide bounds on timing and sensor element localization. To obtain worst case estimates of the impact of these error sources with respect to emitter location, we analyzed emitter location accuracy for a single measurement for a single geometry without the inclusion of iteratively updating the emitter location estimate through subsequent measurements versus increasing numbers of array elements. In the future, we will incorporate the iterative update of the emitter location estimate through subsequent measurements including consideration of dynamic array geometry repositioning. We also intend to add the contributions of other error sources and investigate the use of machine learning methods for a variety of tasks including array repositioning, changing the UAS orientation in-place by its rotation, choosing the number and identifying the sensors for subsequent measurements, and choosing processing parameters and hyperparameters for subsequent measurements – including the adaptive choice of alternative emitter location algorithms.

REFERENCES

[1] S. M. Sheikh, H. M. Asif, K. Raahemifar and F. Al-Turjman, "Time Difference of Arrival Based Indoor Positioning System Using Visible Light Communication," *IEEE Access*, vol. 9, no. 10.1109/ ACCESS.2021.3069793, pp. 52113-52124, 2021.

[2] Texas Instruments, "TI LIDAR Pulsed Time of Flight Reference Design," [Online]. Available: https://www.ti.com/lit/pdf/tiducm1b. [Accessed 03 October 2022].

[3] NOAA, "GPS Accuracy," National Coordination Office for Space-Based Positioning, Navigation, and Timing, 3 March 2022. [Online]. Available: https://www.gps.gov/systems/gps/performance/accuracy/ . [Accessed 10 August 2022].

[4] S. Knappe, V. Shah, P.D.D. Schwindt, L. Hollberg, J. Kitching, L.-A. Liew and J. Moreland, John, "A microfabricated atomic clock". *Applied Physics Letters*. **85** (9): 1460–1462, Aug. 30, 2004.

[5] J. Kitching, "Chip-scale Atomic Devices," *Applied Physics Letters*, **5**(3):031302, 2018.

[6] F. Mekelleche and H. Hafid, "Classification and Comparison of Range-Based Localization Techniques in Wireless Sensor Networks," *Journal of Communications*, vol. 12, no. 10.12720/jcm.12.4.221-227, pp. 221-227, 2017.

[7] S. R. Leelavathy and S. Sophia , "Providing Localization using Triangulation Method in Wireless Sensor Networks," *International Journal of Innovative Technology and Exploring Engineering*, vol. 4, no. 6, pp. 47-50, 2014.

[8] A. Paul and T. Sato, "Localization in Wireless Sensor Networks: A Survey on Algorithms, Measurement Techniques, Applications and Challenges," *Journal of Sensor and Actuator Networks*, vol. 6, no. 4, p. 24, 2017.

[9] M. K. Kumar and V. K. Prasad, "TASLT: Triangular Area Segmentation based Wireless Sensor Network using AoA and RSSI Measures – A New Approach," in proc., *2021 IEEE 18th International Conference on Mobile Ad Hoc and Smart Systems (MASS)*, no. 10.1109/MASS52906.2021.00083, pp. 585-590, 2021. pp. 585-590, 2021.

[10] A. Norrdine, "An Algebraic Solution to the Multilateration Problem," in proc., *2012 International Conference on Indoor Positioning and Indoor Navigation (IPIN)*, 2012.

[11] M. D. Gillete and H. F. Silverman, "A Linear Closed-Form Algorithm for Source Localization from Time-Differences of Arrival," *IEEE Signal Processing Letters*, vol. 15, pp. 1-4, 2008.

[12] S. S. Reddi, "An Exact Solution to Range Computation with Time Delay Information for Arbitrary Array Geometries," *IEEE Transactions on Signal Processing*, vol. 41, no. 1, pp. 485-, 1993.

[13] R. O. Schmidt, "A new approach to geometry of range difference location," *IEEE Transactions on Aerospace and Electronic Systems*, Vols. AES-8, no. 6, pp. 821-835, 1972.

[14] R. O. Schmidt, "Least Squares Range Difference Location," *IEEE Transactions on Aerospace and Electronic Systems,* vol. 32, no. 1, pp. 234-242, 1996.

[15] D. Vasisht, S. Kumar and D. Katabi, "Decimeter-Level Localization with a Single WiFi Access Point," in proc., *13th USENIX Symposium on Networked Systems Design and Implementation*, vol. NSDI 16, pp. 165-178, 2016.

[16] D. Katabi, D. Vasisht and S. S. Kumar, (*inventors*), "Sub-Decimeter Radio Frequency Ranging". *U.S. Patent* 9,961,495, May 1, 2018.

[17] S. Prager, M. S. Haynes and M. Moghaddam, "Wireless Subnanosecond RF Synchronization for Distributed Ultrawideband Software-Defined Radar Networks," *IEEE Transactions on Microwave Theory and Techniques*, vol. 68, no. 11, pp. 4787-4804, 2020.

[18] L. Hollberg and J. Kitching (*inventors*), "Miniature Frequency Standard Based on All-optical Excitation and A Micro-machined Containment Vessel". *U.S. Patent* 6,806,784, Oct. 19, 2004.

[19] Microsemi, "Chip Scale Atomic Clock (CSAC)," Microchip, [Online]. Available: https://www.microsemi.com/product-directory/clocks-frequency-references/3824-chip-scale-atomic-clock-csac. [Accessed 1 October 2022].

[20] L. Zhou, G. Li, Z. Zheng and X. Yang, "TOA Estimation with Cross Correlation-Based Music Algorithm for Wireless Location," in proc., *2014 Fourth International Conference on Communication Systems and Network Technologies*, 2014, pp. 862-865, doi: 10.1109/CSNT.2014.179.

[21] C. Knapp and G. Carter, "The Generalized Correlation Method for Estimation of Time Delay," in proc., *IEEE Trans. Ac., Spch. and Sig. Proc. (ICASSP)*, vol. 44, pp. 320-327, 1976.

[22] M. Azaria and D. Hertz, "Time Delay Estimation by Generalized Cross Correlation Methods," in proc., *IEEE Trans. Ac., Spch. and Sig. Proc. (ICASSP)*, vol. 32, pp. 280-285, 1984.

[23] J. Benesty, C. Jingdong and H. Yiteng, "Time-delay Estimation Via Linear Interpolation and Cross Correlation," *IEEE Trans. Speech and Audio Proc.*, vol. 12, pp. 509-519, 2004.

[24] A. Yeredor, "Analysis of the Edge-effects in Frequency-domain TDOA Estimation," in proc., *2012 IEEE International Conference on Acoustics, Speech and Signal Processing (ICASSP)*, 2012, pp. 3521-3524, doi: 10.1109/ICASSP.2012.6288676.

[25] X. Ning, X. Sha and X. Wu, "A TOA Estimation Method for IR-UWB Ranging Systems," in proc., *2010 First International Conference on Pervasive Computing, Signal Processing and Applications*, 2010, pp. 684-687, doi: 10.1109/PCSPA.2010.170.

[26] J. Xu, Z. Wang, Q. Liu and L. Ren, "A novel TOA estimation method for unknown signal based on intra-pulse correlation accumulation," in proc., *2016 IEEE International Conference on Signal Processing, Communications and Computing (ICSPCC)*, 2016, pp. 1-4, doi: 10.1109/ICSPCC.2016.7753696.

[27] N. Patwari, J. N. Ash, S. Kyperountas, A. O. Hero, R. L. Moses and N. S. Correal, "Locating the Nodes: Cooperative Localization in Wireless Sensor Networks," *Signal Processing Magazine, IEEE*, vol. 22, pp. 54-69, 2005.

[28] D. J. Torrierri, "Statistical Theory of Passive Location Systems," *IEEE Trans. On Aerospace and Electronic Systems*, vol. 20, no. 2, pp. 183-198, 1984.

[29] R. Kaune, J. Hörst and W. Koch, "Accuracy analysis for TDOA localization in sensor networks," in proc., *14th International Conference on Information Fusion*, pp. 1-8, 2011.

[30] S. M. Kay, Fundamentals of Statistical Signal Processing: Estimation Theory, Prentice Hall PTR, 1993.

[31] Y. Wang and K. C. Ho, "TDOA Source Localization in the Presence of Synchronization Clock Bias and Sensor Position Errors," *IEEE Transactions on Signal Processing*, vol. 61, no. 18, pp. 4532-4544, 2013.

BIOGRAPHY

Christopher Peters *received his B.S. and M.S. degrees in physics from the University of Mississippi and his M.S. in Systems Engineering from Johns Hopkins University. He is currently pursuing his PhD with Southern Methodist University, and he is an Electrical Engineer with L3Harris where he develops integration and test strategies for Active Electronically Scanned Array (AESA) systems and components. Prior to L3Harris, he worked with Raytheon Technologies leading Engineering teams in manufacturing & testing of AESA radar systems and developing next-generation technologies for Electronic Warfare & Communications systems for the Department of Defense.*

Mitchell A. (Mitch) Thornton *is currently the Cecil H. Green Chair of Engineering and Professor in the Department of Electrical and Computer Engineering at Southern Methodist University in Dallas, Texas. He also serves as the Executive Director of the Darwin Deason Institute for Cyber Security, a research unit at SMU. His prior industrial experience includes employment at Amoco Research Center, E-Systems, Inc (now L3Harris Communications, Inc.), and the Cyrix Corporation where he held a variety of engineering positions. His research areas include cyber security, applications of data science, signal processing and sensor-based systems in security,*

autonomous systems, and quantum informatics. He is an author or co-author of over 300 technical articles and five books and a named inventor on more than 20 patents and patents pending. He has performed sponsored research for several different government agencies and industrial organizations. He is a licensed professional engineer and he holds a general radiotelephone operator license with radar endorsement from the U.S. Federal Communications Commission. He received the PhD in computer engineering from SMU, MS in computer science from SMU, MS in electrical engineering from the University of Texas at Arlington, and BS in electrical engineering from Oklahoma State University.